ISBN: 978-3-95450-232-5 ISSN: 2673-7000 doi:10.18429/JACoW-NAPAC2022-WEPA01

BEAM DYNAMICS OPTIMIZATION OF A LOW EMITTANCE PHOTOINJECTOR WITHOUT BUNCHER CAVITIES*

J. Qiang†, LBNL, Berkeley, CA, USA
F. Ji, T. Raubenheimer, SLAC, Menlo Park, CA, USA

Abstract

The photoinjector plays an important role in generating high brightness low emittance electron beam for x-ray free electron laser applications. In this paper, we report on beam dynamics optimization study of a low emittance photoinjector based on a proposed superconducting gun without including any buncher cavities. Multi-objective optimization with self-consistent beam dynamics simulations was employed to attain the optimal Pareto front.

INTRODUCTION

The high brightness, coherent x-ray Free Electron Laser (FEL) provides an important tool for scientific discoveries in basic energy science. The LCLS-II-HE as a high energy upgrade of the high repetition rate X-ray FEL, LCLS-II [1, 2], will increase the final electron beam energy from 4 GeV to 8 GeV and photon spectral range to 12.8 keV with a potential to be extended through 20 keV [3]. In order to attain the 20 keV shorter wavelength x-ray radiation using the 8 GeV electron beam, a low emittance injector based on a 185 MHz superconducting RF (SRF) gun [4], one or two buncher cavities, and a superconducting RF cryomodule of boosting cavities has been actively pursued [5]. In this paper, we explored an alternative design of the low emittance injector without using any buncher cavities. Figure 1 shows the schematic layout of such an injector. The photo-electron beam out of the SRF gun is focused by a solenoid and accelerated by eight 1.3 GHz superconducting boosting cavities. Such an injector has a simpler structure and lower cost than the nominal design. The disadvantage of this injector is lack of flexibility.

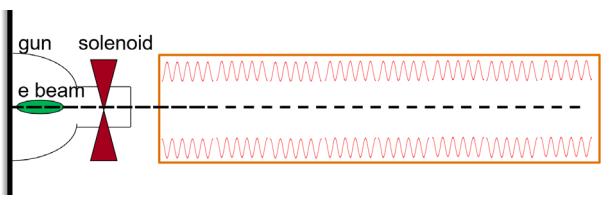

Figure 1: Schematic layout of the low emittance photoinjector.

MULTI-OBJECTIVE BEAM DYNAMICS OPTIMIZATION METHOD

A multi-objective optimization algorithm based on the differential evolution with varying population size and external storage was used in study [6]. In this method, the population size varies from one generation to next generation. Only nondominated solutions are kept in the population of each generation. Here, the nondominated solution is a solution that at least one component (i.e. one objective function) of this solution is better than the same component of all other solutions. An external storage is used to save all nondominated solutions from previous generations. The next generation parent solutions are selected from both the present generation offspring solutions and the external stored solutions. The advantage of using a variable population size with external storage is to reduce the number of objective function evaluations and to improve the speed of convergence. The new algorithm is summarized in the following steps: (i) Step 0: Define the minimum parent size, NP_{min} and the maximum size, NP_{max} of the parent population. Define the maximum size of the external storage, NP_{ext}. (ii) Step 1: An initial NP_{ini} population of parameter vectors are chosen quasi-randomly to cover the entire solution space. (iii) Step 2: Generate the offspring population using a unified differential evolution algorithm. (iv) Step 3: Check the new population against the constraints. (v) Step 4: Combine the new population with the existing parent population from the external storage. Nondominated solutions (NP_{ndom}) are found from this group of solutions and min(NP_{ndom}, Next) of solutions are put back to the external storage. Pruning is used if $NP_{ndom} > NP_{ext}$. NP parent solutions are selected from this group of solutions for next generation production. If $NP_{min} \le NP_{ndom} \le NP_{max}$, $NP = NP_{ndom}$. Otherwise, $NP = NP_{min}$ if $NP_{ndom} < NP_{min}$ and $NP = NP_{max}$ if $NP_{ndom} > NP_{max}$. The elitism is emphasized through keeping the nondominated solutions while the diversity is maintained by penalizing the overcrowded solutions through pruning. (vi) Step 5: If the stopping condition is met, stop. Otherwise, return to Step 2. The differential evolution method is used to generate new trial solutions from the parent solutions. This method makes use of the difference between the current solution and best solution to emulate the gradient information and the difference of two randomly selected solutions and mutation to enhance the diversity of the solution [7, 8]. The differential evolution method as a simple but powerful method has been widely used in many applications. This multi-objective evolutionary optimizer is integrated with a parallel beam dynamics simulation code, IMPACT-T [9], to optimize the final electron beam quality at the exit of the injector. The IMPACT-T code is a three-dimensional macroparticle tracking code based on the particle-in-cell method. It simulates the electron beam emission from the photocathode and the electron beam transport and acceleration through the injector including the self-consistent space-charge effects. Here, the space-charge effects were computed by solving the three-dimensional Poisson equation in the beam frame using an integrated Green's function method. The fast Fourier transform

* Work supported by the Director of the Office of Science of the US Department of Energy under Contract no. DEAC02-05CH11231.
† jqiang@lbl.gov

ISBN: 978-3-95450-232-5 ISSN: 2673-7000 doi:10.18429/JACoW-NAPAC2022-WEPA01

(FFT) is used to compute the discrete convolution efficiently. The electron beam properties such as transverse emittance and longitudinal Root Mean Square (RMS) bunch length at the exit of the injector from the IMPACT-T simulation are used as objective functions of the optimizer.

OPTIMIZATION RESULTS

Table 1: Control Parameters Used in Optimization

Parameters	Range	Unit
Laser spot size	(0.14, 0.56)	mm
Laser pulse length	(20.0, 81.0)	ps
SRF gun phase	(150.0, 190.0)	degree
Solenoid field amp.	(0.082, 0.33)	Tesla
Starting location	(0.5, 2.0)	m
Cavity 1 field amp.	(0, 32.0)	MV/m
Cavity 1 phase	(0, 360)	degree
Cavity 2 field amp.	(0, 32.0)	MV/m
Cavity 2 phase	(0, 360)	degree
Cavity 3 field amp.	(0, 32.0)	MV/m
Cavity 3 phase	(0, 360)	degree
Cavity 4 field amp.	(17.5, 32.0)	MV/m
Cavity 4 phase	(0, 360)	degree

Multi-objective beam dynamics optimizations were carried out for the injector layout shown in the Fig. 1 without any buncher cavities. Here, we defined two objective functions at the exit of the injector: transverse RMS projected emittance and longitudinal RMS bunch length. The longitudinal RMS bunch length is a measure of final peak current: the shorter the bunch length, the higher the peak current. In this study, we used 13 control knobs in the injector to optimize the final electron beam properties. These control knobs are listed in Table 1 with corresponding range used in the optimization. The rest four RF cavities (5-8) inside the boosting cryomodule run on the crest with a maximum 32MV/m electric field on the axis.

The electric field amplitude at the cathode has significant impact on the final electron beam quality. A higher electric field results in a faster acceleration and mitigation of the strong space-charge effects near the cathode. The superconducting RF gun used in this study is similar to the WiFEL superconducting gun [10]. The design goal of this gun is to attain 30MV/m electric field at the cathode. Figure 2 shows the Pareto front of the final RMS bunch length and RMS projected emittance using 0.6 um/mm and 1 um/mm initial thermal emittance corresponding to 184 meV and 511 meV mean transverse energy respectively. It is seen that with an assumption of 0.6 um/mm thermal emittance, the final transverse RMS emittance can be less than 0.1 um with an RMS bunch length about 1 mm, which corresponds to a peak current around 10 A. For a 1 um/mm thermal emittance, the transverse emittance is about 0.13 um with 1 mm RMS bunch length. The larger thermal emittance results in larger final transverse emittance for the same bunch length and longer bunch length (lower current) for the same transverse emittance at the injector exit.

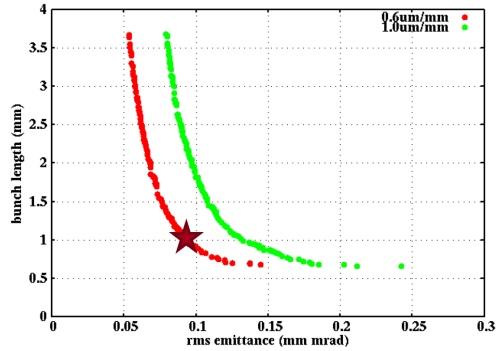

Figure 2: Pareto front of the final RMS bunch length and transverse RMS projected emittance with 0.6 um/mm (red) and 1 um/mm (green) thermal emittance and 30MV/m electric field at the cathode.

The 30 MV/m electric field at the cathode in the SRF gun is the design target. To check the impact of the lower electric field on the electron beam quality, we also carried out beam dynamics optimization using 20 MV/m electric field at the cathode. Figure 3 shows the Pareto front of the final transverse RMS emittance and RMS bunch length at the exit of the injector after the beam dynamics optimization. Assuming an initial 0.6 um/mm thermal emittance, the final RMS bunch length reaches more than 3 mm in order to attain 0.1 um final transverse emittance. This shows that the electric field at the cathode can have significant impact on the final electron beam quality.

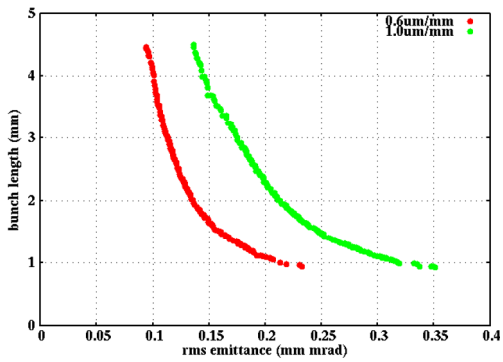

Figure 3: Pareto front of the final RMS bunch length and transverse RMS projected emittance with 0.6 um/mm (red) and 1 um/mm (green) thermal emittance and 20MV/m electric field at the cathode.

In the above beam dynamics optimizations, we assumed that the variation of the starting location of the boosting cryomodule. This might not be valid since once the location is selected for one optimization results based on the 30 MV/m nominal design parameter, it is no longer moveable for the 20 MV/m optimization. To check the effect of this location on the final beam quality, we redid the beam dynamics optimization of 20 MV/m case with only 12 control knobs and a fixed boosting cryomodule starting location

ISBN: 978-3-95450-232-5 ISSN: 2673-7000 doi:10.18429/JACoW-NAPAC2022-WEPA01

from a solution of the 30MV/m optimization. Figure 4 shows the Pareto front of the final transverse emittance and bunch length with 13 and 12 control knobs and 0.6 um/mm thermal emittance. The final Pareto fronts are similar in both cases. This shows that one can use the physical element layout from the 30 MV/m beam dynamics optimization, and set the laser parameters and amplitudes and phases of the cavity and solenoid fields for the 20 MV/m cathode electric field to achieve an optimal final beam quality.

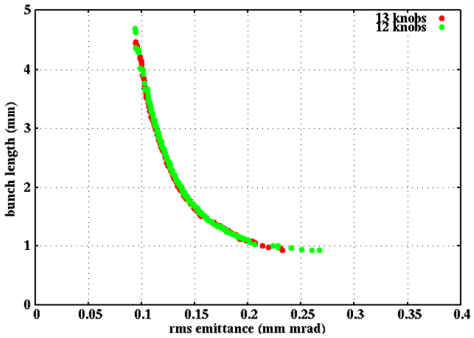

Figure 4: Pareto front of the final RMS bunch length and transverse RMS projected emittance with 13 control knobs (red) and 12 control knobs (green) and 0.6 um/mm and 20MV/m electric field at the cathode.

To see the electron beam evolution through the low emittance photoinjector, we selected one optimal solution from the Pareto front shown as star in the Fig. 2. Figure 5

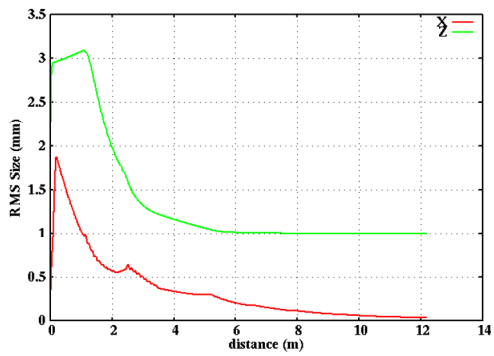

Figure 5: RMS transverse size (red) and longitudinal bunch length (green) evolution through the photoinjector for the star solution in Figure 2.

shows the RMS transverse size and bunch length evolution through the injector. It is seen that the electron beam is first transversely focused by the solenoid magnet and then further focused by the boosting RF cavities through the injector. With the absence of buncher cavities, the electron beam is longitudinal bunched by the first and the second boosting cavities and is longitudinally frozen through the rest of the injector after the electron energy is over 10 MeV. Figure 6 shows the transverse RMS projected emittance evolution through the injector. The transverse emittance goes down through the solenoid and the boosting cavities and freezes after the first four cavities. The final transverse emittance is less than 0.1 um. For the majority core part of the beam, the slice emittance is less than 0.09 um.

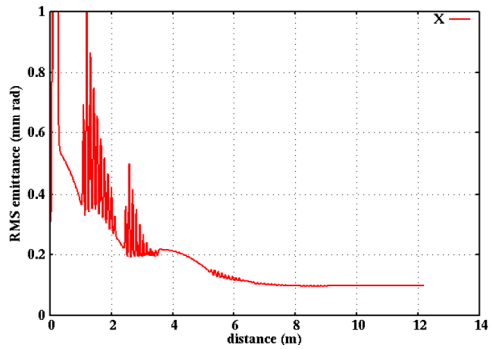

Figure 6: RMS transverse projected emittance evolution through the low emittance photoinjector.

Figure 7 shows the final longitudinal phase space distribution and current profile of the electron beam at the injector exit. The final RMS energy spread is about 1% with the peak current of 13 A.

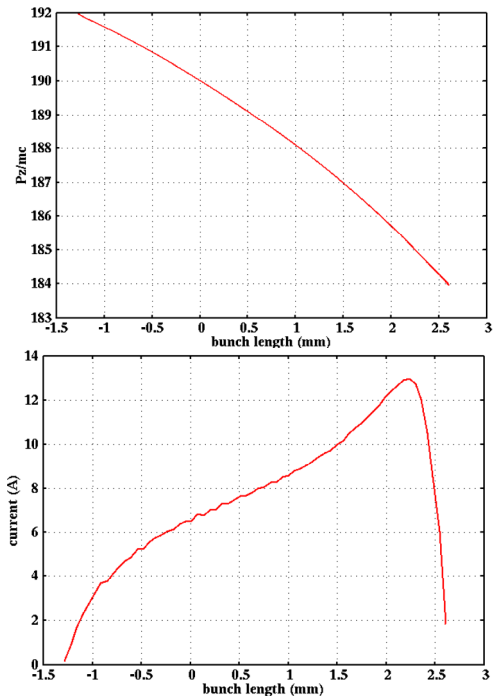

Figure 7: Final longitudinal phase space distribution (top) and current profile (bottom) for the star solution in Figure 2.

DISCUSSIONS

In this study, we applied multi-objective optimizations to a photoinjector beam dynamics design without any buncher cavities to attain a final low emittance beam. Such an injector simplifies the injector design and operation, and also has a lower cost. The issue of this injector has less control knobs (less flexible) compared with the design with one and two buncher cavities. Furthermore, the optimized distance from the starting location of the boosting cryomodule to the photocathode is too short to fit into the current LCLS-II-HE low emittance injector design.

ISBN: 978-3-95450-232-5 ISSN: 2673-7000 doi:10.18429/JACoW-NAPAC2022-WEPA01

REFERENCES

[1] T.O. Raubenheimer, "LCLS-II: Status of the CW X-ray FEL upgrade to the LCLS facility", in *Proc. FEL'15*, Daejeon, Korea, Aug. 2015, paper WEP014, pp. 618-624.

[2] LCLS-II Conceptual Design Report, SLAC-R-1092, http://slac.stanford.edu/pubs/slacreports/reports09/slac-r-1092.pdf

[3] T.O. Raubenheimer, "The LCLS-II-HE, A high energy upgrade of the LCLS-II", in *Proc. FLS'18*, Shanghai, China, Mar. 2018, pp. 6-11. doi:10.18429/JACoW-FLS2018-MOP1WA02

[4] J. Lewellen *et al*., "Status of the SLAC/MSU SRF gun development project," presented at NAPAC'22, Albuquerque, NM, USA, Aug. 2022, paper WEPA03, this conference.

[5] F. Ji, C. Adolphsen, R. Coy, L. Ge, C. E. Mayes, T. O. Raubenheimer, M. C. Ross, X. J. Wang, L. Xiao, F. Zhou and S. T. Littleton, "Beam dynamics studies on a low emittance injector for LCLS-II-HE," presented at NAPAC'22, Albuquerque, NM, USA, Aug. 2022, paper WEPA02, this conference.

[6] J. Qiang, "Advances in global optimization of high brightness beams," *International Journal of Modern Physics A*, vol. 34, 1942016, 2019. doi:10.1142/S0217751X19420168

[7] R. Storn and K. Price, "Differential evolution – A simple and efficient heuristic for global optimization over continuous spaces," *J. Global Optim*. 11, p. 341, 1997.

[8] J. Qiang, C. Mitchell and A. Qiang, "Tuning of an adaptive unified differential evolution algorithm for global optimization," in *Proc. CEC2016*, Vancouver, Canada, Jul. 2016, p. 4061. doi:10.1109/CEC.2016.7744305

[9] J. Qiang, S. Lidia, R. D. Ryne and C. Limborg-Deprey, "Three-dimensional quasistatic model for high brightness beam dynamics simulation," *Phys. Rev. ST Accel. Beams*, vol. 9, 044204 (2006).

[10] R. A. Legg *et al*., "Status of the Wisconsin SRF gun", in *Proc. IPAC'12*, New Orleans, LA, USA, May 2012, paper MOPPP045, pp. 661-663.